JOURNAL OF VIROLOGY, Oct. 2002, p. 9962–9971 Vol. 76, No. 19
0022-538X/02/$04.00+0 DOI: 10.1128/JVI.76.19.9962–9971.2002

Intact Microtubules Support Adenovirus and Herpes Simplex Virus Infections

Hélène Mabit,[1] Michel Y. Nakano,[1] Ute Prank,[2] Bianca Saam,[1] Katinka Döhner,[2] Beate Sodeik,[2] and Urs F. Greber[1]*

Zoologisches Institut, Universität Zürich, CH-8057 Zürich, Switzerland,[1] and Zentrum für Biochemie, Medizinische Hochschule Hannover, D-30623 Hannover, Germany[2]

Received 10 April 2002/Accepted 18 June 2002

Capsids and the enclosed DNA of adenoviruses, including the species C viruses adenovirus type 2 (Ad2) and Ad5, and herpesviruses, such as herpes simplex virus type 1 (HSV-1), are targeted to the nuclei of epithelial, endothelial, fibroblastic, and neuronal cells. Cytoplasmic transport of fluorophore-tagged Ad2 and immunologically detected HSV-1 capsids required intact microtubules and the microtubule-dependent minus-end-directed motor complex dynein-dynactin. A recent study with epithelial cells suggested that Ad5 was transported to the nucleus and expressed its genes independently of a microtubule network. To clarify the mechanisms by which Ad2 and, as an independent control, HSV-1 were targeted to the nucleus, we treated epithelial cells with nocodazole (NOC) to depolymerize microtubules and measured viral gene expression at different times and multiplicities of infections. Our results indicate that in NOC-treated cells, viral transgene expression was significantly reduced at up to 48 h postinfection (p.i.). A quantitative analysis of subcellular capsid localization indicated that NOC blocked the nuclear targeting of Ad2 and also HSV-1 by more than 90% at up to 7 h p.i. About 10% of the incoming Texas Red-coupled Ad2 (Ad2-TR) was enriched at the nucleus in microtubule-depleted cells at 5 h p.i. This result is consistent with earlier observations that Ad2-TR capsids move randomly in NOC-treated cells at less than 0.1 μm/s and over distances of less than 5 μm, characteristic of Brownian motion. We conclude that fluorophore-tagged Ad2 and HSV-1 particles are infectious and that microtubules play a prominent role in efficient nuclear targeting during entry and gene expression of species C Ads and HSV-1.

Many viruses, including adenoviruses (Ads) and herpesviruses, spread by intracellular transport within infected host cells, thus increasing the viral load in target organs and possibly causing severe disease (44). The 51 human Ad serotypes—classified into six species (A to F)—have distinct tropisms (19). For example, Ad type 2 (Ad2) and Ad5 (species C) and Ad3 (species B) are associated with upper-airway infections. Other serotypes are linked to epidemic keratoconjunctivitis (species D), pneumonia (species E), enteric infections (species A and F), or infections of hematopoietic cells (41). The *Herpesviridae* family consists of the alpha-, beta- and gammaherpesviruses. Like Ads, alphaherpesviruses, including herpes simplex virus type 1 (HSV-1), infect different cell types both in cultures and in their hosts. After infection of mucosal or damaged cutaneous epithelium, these neurotropic viruses establish latent infections, primarily in sensory ganglia, that, upon reactivation, lead to recurrent epidermal lesions (40, 55). The ability to infect a broad range of postmitotic cells has made both Ads and herpesviruses useful gene delivery vehicles (21) that are currently being evaluated in clinical trials (29, 39). For their application as therapeutic vectors and to identify new potential targets for antiviral therapy, it is crucial to understand how the genomes are targeted to the nucleus.

The entry mechanisms for Ads and herpesviruses have been well studied. Ads are internalized by receptor-mediated endocytosis that is dependent on F actin and leave the endosomal pathway at various sites (recently reviewed in reference 11). The species C Ads, including Ad2 and Ad5, exit from a slightly acidic compartment of pH 6 at about 10 min postentry (16, 42), whereas Ad7 (species B) has been reported to escape from acidic late endosomes and lysosomes (32). In contrast, HSV-1 delivers its capsids into the cytosol upon fusion of the viral envelope with the plasma membrane (45, 46). Both viruses then target their capsids to the cell nucleus, uncoat, and inject the enclosed linear double-stranded DNA genomes through the nuclear pores into the nucleoplasm for replication (14, 35, 53).

A number of electron microscopy studies have shown that cytoplasmic capsids of both species C Ads and alphaherpesviruses can associate with microtubules (MTs) (5, 10, 27, 28, 31, 37, 45, 47, 57). Moreover, time-lapse fluorescence microscopy experiments of fluorophore-tagged Ads have demonstrated that Ads move along linear tracks of MTs (25, 26, 49). The motility of incoming particles is bidirectional, toward and away from the nucleus, but the overall motilities are toward the minus ends of MTs and require the major minus-end-directed motor dynein and the cofactor dynactin. If MTs are depolymerized with nocodazole (NOC), then the long-range linear motilities cease, the remaining short-range transport has no directional control and, most importantly, the efficiency of Ad2 DNA delivery is strongly reduced, as indicated by fluorescence in situ hybridization assays (48, 49).

Similar results have been reported for alphaherpesviruses.

* Corresponding author. Mailing address: Zoologisches Institut der Universität Zürich, Winterthurerstr. 190, CH-8057 Zürich, Switzerland. Phone: 41 1 635 4841. Fax: 41 1 635 6822. E-mail: ufgreber@zool.unizh.ch.

MT-depolymerizing agents block HSV-1 infections in cultures and in animal models (17, 22, 45, 51, 52). Moreover, incoming HSV-1 capsids colocalize with dynein and dynactin, and transport to the nucleus is reduced by the dynein inhibitors erythro-9[3-(2-hydroxynonyl)]adenine and dynamitin (6a, 22, 45). Axonal herpesvirus transport occurs at rates of 0.5 to 3.5 μm/s, with peak velocities of up to 5 μm/s (1, 28, 37, 43); viral structures are transported bidirectionally along linear tracks with high processivity over distances of up to 20 μm, as demonstrated by video microscopy with green fluorescent protein (GFP)-tagged mutants (1, 43; A. Wolfstein et al., unpublished data).

In a recent article, it was proposed that Ad5 infections do not require MTs (8). We therefore decided to conduct a quantitative analysis of Ad5-mediated gene expression and Texas Red (TR)-coupled Ad2 (Ad2-TR) subcellular localization in cells depleted of MTs; as an independent control, we included HSV-1. Our results show that the large majority of Ad2-TR, Ad5, and HSV-1 particles utilize intact MTs to reach the nucleus in order to infect nonpolarized epithelial cells.

MATERIALS AND METHODS

Cells and reagents. Immortalized human adenocarcinoma-derived alveolar epithelial A549 cells (ATCC CCL-185) were maintained in Dulbecco's modified Eagle's medium (Gibco Invitrogen, Basel, Switzerland) containing 7% Clone III serum (HyClone; Socochim, Geneva, Switzerland) and 1% nonessential amino acids, 2 mM glutamine, 100 U of penicillin/ml, and 0.1 mg of streptomycin/ml (all from Gibco-BRL). PtK_2 cells (ATCC CCL-56) and BHK-21 cells (ATCC CCL-10) were grown in 10% and Vero cells (ATCC CCL-81) were grown in 7.5% fetal calf serum containing minimal essential medium, 2 mM glutamine, nonessential amino acids and, for Vero cells, 100 U of penicillin/ml and 100 μg of streptomycin/ml. All cell lines were cultured in a humidified 5% CO_2–air atmosphere. NOC (Sigma) and paclitaxel (Calbiochem-Novabiochem or Sigma) were dissolved as 1,000-fold stocks in dimethyl sulfoxide (DMSO) and used as indicated below. For the immunofluorescence experiments, we used preadsorbed rabbit polyclonal antibodies raised against DNA-containing capsids (anti-heavy chain [HC]) or empty capsids (anti-light chain [LC]) to detect incoming viral capsids (4, 45). MTs were labeled with a mouse monoclonal antibody against β-tubulin (N357; Amersham, Little Chalfont, United Kingdom) (2).

Ad infection and gene expression. Ad2 was purified and coupled to TR as described previously to yield Ad2-TR (33). This virus was as infectious as the nonlabeled parent virus, as determined by plaque assays with A549 cells. The Ad5 derivative AE18, lacking the E1 and E3 regions, expressed *lacZ* from the cytomegalovirus (CMV) major promoter (provided by E. Vigne, Institut G. Roussy, Villejuif, France) (54). Luc-Ad5, lacking E1 and E3, expressed luciferase from a CMV promoter inserted into the E1 region (kindly provided by S. Hemmi and D. Serena, University of Zürich). In brief, this virus was constructed from a pPoly plasmid backbone (3) and plasmid pTG-H5 DL324 (kindly supplied by S. Rusconi, University of Fribourg, Fribourg, Switzerland). Cells were seeded in 24-well dishes (Costar; Integra Biosciences) or on glass coverslips 1 to 2 days before the experiment. Prior to infection, 60 to 90% confluent cells were exposed to NOC in DMSO or just DMSO alone in Dulbecco's modified Eagle's medium for 1 h and then were infected with AE18 at 100 to 10,000 physical particles per cell at 37°C. At various times after the addition of the virus, cells were either analyzed for their viability or lysed, and lysates were assayed for β-galactosidase (β-Gal) activity and protein content. β-Gal activity was measured by a β-Gal enzyme assay (Promega Corporation). The cells in 1 well of a 24-well dish were washed with phosphate-buffered saline (PBS) at 7, 24, 32, or 48 h postinfection (p.i.) and lysed in 400 μl of reporter lysis buffer (Promega) for 15 min at room temperature under slowly rocking conditions. The lysates were centrifuged in a microcentrifuge at 4°C for 2 min, and 30 μl of the supernatants was mixed with the same volume of 2× enzyme reaction buffer (Promega) and incubated at 37°C for various times. The reactions were stopped by the addition of 100 μl of 1 M sodium carbonate. The absorbance was read at 420 nm with a spectrophotometer (MRX microplate reader; Dynatech Laboratories; BioLogics, Gainesville, Va). The background activity of noninfected A549 cells was subtracted from the measurements. The protein content of each lysate was measured with Micro BCA protein assay reagent (Pierce), and the results are expressed as enzymatic units per milligram of protein per minute. The luciferase activity of infected cells was determined with cell lysates at 7 h p.i. by using a commercial assay system (Promega). The cells in 1 well of a 24-well dish were washed with PBS and lysed in 400 μl of reporter lysis buffer. The centrifuged lysates (20 μl) were placed in an opaque 96-well plate for luciferase activity measurements with a Multilabel Counter (Wallac Victor^2 1420; Perkin-Elmer), which injected 50 μl of luciferase assay reagent into each well.

HSV-1 infection and gene expression. Wild-type HSV-1 strain F (ATCC VR-733) and mutant strain [KOS]tk12 were amplified and purified as described previously (45). Immediate-early viral gene expression was analyzed by using mutant [KOS]tk12, which lacks the viral thymidine kinase gene and encodes the enzyme β-Gal under the control of the immediate-early ICP4 promoter of HSV-1 (kindly provided by P. Spear, Northwestern University, Chicago, Ill.) (56). PtK_2 cells were cultured in 24-well plates at a density of 4×10^4 to 5×10^4 cells per well for 1 day. They were pretreated with NOC or paclitaxel in DMSO or just DMSO alone for 1 h, cooled to 4°C, and incubated with virus for 2 h as described elsewhere (6a, 45). Unbound virus was removed by repeated washing in PBS, and the cells were further incubated in culture medium at 37°C.

At different times, the cells were lysed with 0.5% Triton X-100 (TX-100) in PBS containing 1 mg of bovine serum albumin/ml and protease inhibitors at 37°C for 15 min. Lysates were then incubated with 3.5 mg of *o*-nitrophenyl-β-D-galactopyranoside/ml in 73 mM Na_2HPO_4–16 mM NaH_2PO_4–0.2 mM KH_2PO_4–0.4 mM KCl–17 mM NaCl. The enzymatic activity of β-Gal was measured after about 2 h at 420 nm by using a plate reader (Spectra Count microplate photometer; Packard Instrument Company, Meriden, Conn.). On a parallel plate, cells were fixed with 3% (wt/vol) paraformaldehyde (PFA) in PBS for 20 min, washed with water, and then stained with 0.25 mg of crystal violet/ml in 5% ethanol for 10 min to quantify the amount of cells present after different treatments. After several washes in water, the plates were dried, and the bound crystal violet was dissolved in 100% ethanol and quantified by measuring the optical density at 590 nm (17). Crystal violet staining gave a linear signal over cell concentrations ranging from at least 3×10^3 to 3×10^5 cells per well (data not shown).

Quantification of subcellular viral targeting. To analyze the subcellular distribution of incoming HSV-1 capsids, Vero or PtK_2 cells were infected in the presence of 0.5 mM cycloheximide. The cells were then (i) fixed with 100% methanol for 4 min at −20°C after a 10-s preextraction in 0.5% TX-100–80 mM PIPES-KOH (pH 6.8)–2 mM $MgSO_4$–10 μM paclitaxel to visualize MTs and capsids as described previously (45), (ii) fixed and permeabilized simultaneously with PHEMO-fix (3.7% [wt/vol] PFA, 0.05% [wt/vol] glutaraldehyde, and 0.5% TX-100 in PHEMO-buffer [see below]) for 10 min and washed with PHEMO-buffer (68 mM PIPES-KOH [pH 6.9], 15 mM EGTA, 3 mM $MgCl_2$, 10% DMSO) to label MTs, or (iii) fixed with 3% (wt/vol) PFA in PBS for 20 min and then permeabilized with 0.1% (vol/vol) TX-100 for exactly 5 min. The remaining PFA was inactivated by incubating the cells with 50 mM NH_4Cl–PBS for 10 min. Immunolabeling was performed as described elsewhere (6a, 45). The cells were examined either with a modified confocal microscope (model MRC600; Bio-Rad Laboratories, Hercules, Calif.) attached to an Axiovert microscope (Carl Zeiss, Inc., Thornwood, N.Y.) with separate filters for each fluorochrome or with a Leica SP1 microscope (×63 oil-immersion objective; numeric aperature, 1.32) with UV excitation at 351 and 364 nm and with fluorescein isothiocyanate (468 nm), TR (568 nm), and long-pass emission filters in sequential recording mode at a section thickness of 0.5 μm. Images were processed with Photoshop 5.0 (Adobe). The subcellular distributions of Ad2-TR and HSV-1 (immunolabeled with an anti-LC antibody) were determined by quantitative fluorescence microscopy of cells fixed with PHEMO-fix by the procedure described earlier (33).

Cell viability assay. Cell viability was assessed with a live/dead viability/cytotoxicity two-color fluorescence assay (L-3224; Molecular Probes). This assay measures intracellular esterase activity with the cell-permeable substrate Calcein-AM, which is converted by live cells to the fluorescent polyanion calcein (excitation, 495 nm; emission, 515 nm), which is retained in living cells by the intact plasma membrane. In addition, we used the non-cell-permeating DNA dye ethidium homodimer-1 (EthD-1) (excitation, 495 nm; emission, 635 nm), which is detected in cells with compromised membranes, i.e., dead cells. In this assay, live cells have a green fluorescent cytoplasm but no EthD-1 signal, whereas dead cells lack green fluorescence and are stained with EthD-1. The assays were performed by washing cells once with PBS and incubating them with Calcein-AM (0.8 μM for A549 cells and 0.2 μM for PtK_2 cells) and EthD-1 (0.8 μM for A549 cells and 0.1 μM for PtK_2 cells) in Hanks' medium (Gibco-BRL) at 37°C for 15 min. Cells were washed with Hanks' medium, and fluorescence was analyzed with a Leica inverted fluorescence microscope equipped with a ×63 oil-immersion objective (numeric aperture, 1.32), a band-pass excitation filter, and a double-pass emission filter as described earlier (49). Images were recorded with Meta-

Morph software (Universal Imaging Corporation) and batch processed with Photoshop 5.0.

RESULTS

Glotzer et al. (8) recently suggested that Ad5 infection of the epithelial cell line A549 occurred in the absence of MTs (8), contradicting earlier results (26, 49). A reexamination of the role of MTs in Ad infection was therefore warranted.

NOC is an inhibitor of Ad5 infection. We first analyzed adenovirus transgene expression in A549 cells containing intact or disrupted MTs. Cells were preincubated with different concentrations of the MT-depolymerizing agent NOC at 37°C for 60 min (20) and then were inoculated with β-Gal-expressing Ad5 (β-Gal–Ad5) at 10,000 physical particles per cell, equivalent to about 300 associated particles per cell (48). The particle-to-PFU ratio is estimated to be on the order of 20 to 100, corresponding to 3 to 15 bound infectious particles per cell (18). β-Gal activity was measured in cell lysates at 7 h p.i., the earliest time point that gave a reliable reading. The lowest concentration of NOC (0.2 μM) had no effect on β-Gal expression, whereas 2 μM NOC resulted in 40% inhibition and 20 μM NOC resulted in greater than 80% inhibition compared to the results obtained for untreated cells (Fig. 1A). The latter conditions are sufficient to completely depolymerize MTs in Vero cells (45) (Fig. 4A, panel d), HeLa cells (49), or A549 cells (Fig. 2A, panel e), whereas PtK_2 cells require 50 μM NOC (data not shown). A549 cells were therefore treated with 20 μM NOC, and β-Gal activity was measured at 7, 24, and 48 h after inoculation with 1,000 and 10,000 particles per cell. In both instances, there was a severe reduction of gene expression, with 85% inhibition at 7 h p.i. and 50 to 70% inhibition at 24 and 48 h p.i. (Fig. 1B). The effect of NOC was reversible, as indicated by washing the cells with drug-free medium at 180 min p.i. and incubating them for another 4 h in the absence of drug (Fig. 1C). When NOC was added at 3 h p.i., when a large fraction of the incoming DNA had been delivered to the nucleoplasm (49, 53), there was only marginal inhibition of viral gene expression. This result indicated that most of the infectious particles had reached the nucleus at 3 h p.i. In contrast, when NOC was present throughout the infection, β-Gal expression was reduced by 85% compared to that in control cells.

We next tested the effect of NOC on the gene expression of a different virus, Luc-Ad5. This strategy enabled us to reduce the viral load to 10 particles per cell and still measure transgene activity as early as 7 h p.i. Consistent with the β-Gal activity results, 20 μM NOC reduced luciferase activity by 50 to 70% at 10, 100, 1,000, or 10,000 particles per cell (Fig. 1D). Importantly, the assay was linear in this range. We next analyzed whether NOC affected the viability of the cells either in the presence or in the absence of β-Gal–Ad5. Cells were pretreated with NOC (20 μM) for 1 h, infected or not infected with Ad5, and then stained with the vital dyes Calcein-AM and EthD-1. Intact live cells excluded EthD-1 and cytosolic esterases hydrolyzed Calcein-AM, thus generating green fluorescent Calcein. All cells on the coverslip were EthD-1 negative and Calcein positive (Fig. 1E, panels a to f), unlike cells that had been treated with methanol (Fig. 1E, panels g to i). Importantly, there was no cell loss from the coverslips, as verified by differential interference contrast imaging (Fig. 1E, panels c, f, and i).

NOC blocks the nuclear accumulation of Ad2-TR. If NOC is an early inhibitor of Ad5 infection, then it could have an effect on genome trafficking. To visualize cytoplasmic particles, we used fluorescent Ad2-TR containing two to four TR molecules per hexon trimer, corresponding to 200 to 400 TR molecules per virion (13, 33). Importantly, this virus is as infectious as unlabeled virus and is not aggregated, as judged by electron microscopy of negatively stained particles and population analysis of viral fluorescence (33). A recent study showed that the DNA genome of purified Ad2 separates from the capsid at the nuclear pore complex (NPC) and that the remainder of the capsid tends to form aggregates or becomes undetectable (53). A549 cells were treated with different concentrations of NOC as described above, and Ad2-TR was bound to the cell surface at 4°C for 1 h to synchronize the infection at 37°C in the presence or in the absence of the drug. One set of cells was fixed at 75 min p.i. and stained for MTs. Clearly, increasing amounts of NOC progressively depolymerized MTs (Fig. 2A), whereas DMSO alone had no effect on the morphology of the MT network. By use of a fast Fourier transformation algorithm, viral fluorescence was quantitated in the cell periphery, the cytoplasmic area, and the nucleus, including a perinuclear region of 1.5 μm (33). While control cells had low peripheral and cytoplasmic but high nuclear fluorescence signals (less than 1 but more than 5 fluorescence units per unit area, respectively), 20 μM NOC-treated cells showed almost no nuclear accumulation of Ad2-TR (1.6 fluorescence units per unit area); instead, there was a significant increase in the peripheral and cytoplasmic fluorescence intensity ($P < 0.01$) (Fig. 2B).

We next carried out a time course experiment either in the absence or in the presence of 20 μM NOC. As expected, the nuclear and perinuclear fluorescence of control cells increased to greater than 5 fluorescence units per unit area at 75 min p.i. compared to 1 unit at 0 min p.i., while the peripheral and cytoplasmic Ad2-TR fluorescence decreased to less than 0.2 unit (Fig. 2C). At 150 min, however, the viral capsid load in the nuclear and perinuclear area decreased to less than two, indicative of viral disassembly, which peaks at between 150 and 180 min p.i. (14, 53). The strong decrease in nuclear Ad2-TR particles coincided with a robust increase in peripheral and cytoplasmic virus, suggesting that viral capsids or fragments were transported back to the periphery. Interestingly, the nuclear fluorescence increased again at 300 and 420 min p.i. ($P = 0.05$) and the peripheral fluorescence decreased. These results suggested a second transport wave of Ad2-TR toward the nucleus. This experiment confirms that in control cells, our measurements of fluorescent capsids are quantitative at least until 75 min p.i., the onset of capsid disassembly.

The subcellular virus distribution in NOC-treated cells was fundamentally different from that in control cells. At up to 150 min p.i., the viral capsid load in the nuclear and perinuclear region was no different from the charge at 0 min p.i.; i.e., there was no enrichment of Ad2-TR near the nucleus (Fig. 2D). The virus concentrations in the cytoplasm and the periphery were slightly reduced. Interestingly, we found a small but significant accumulation of Ad2-TR near the nucleus ($P < 0.01$) at 300 min p.i. Approximately 10% of the viral fluorescence appar-

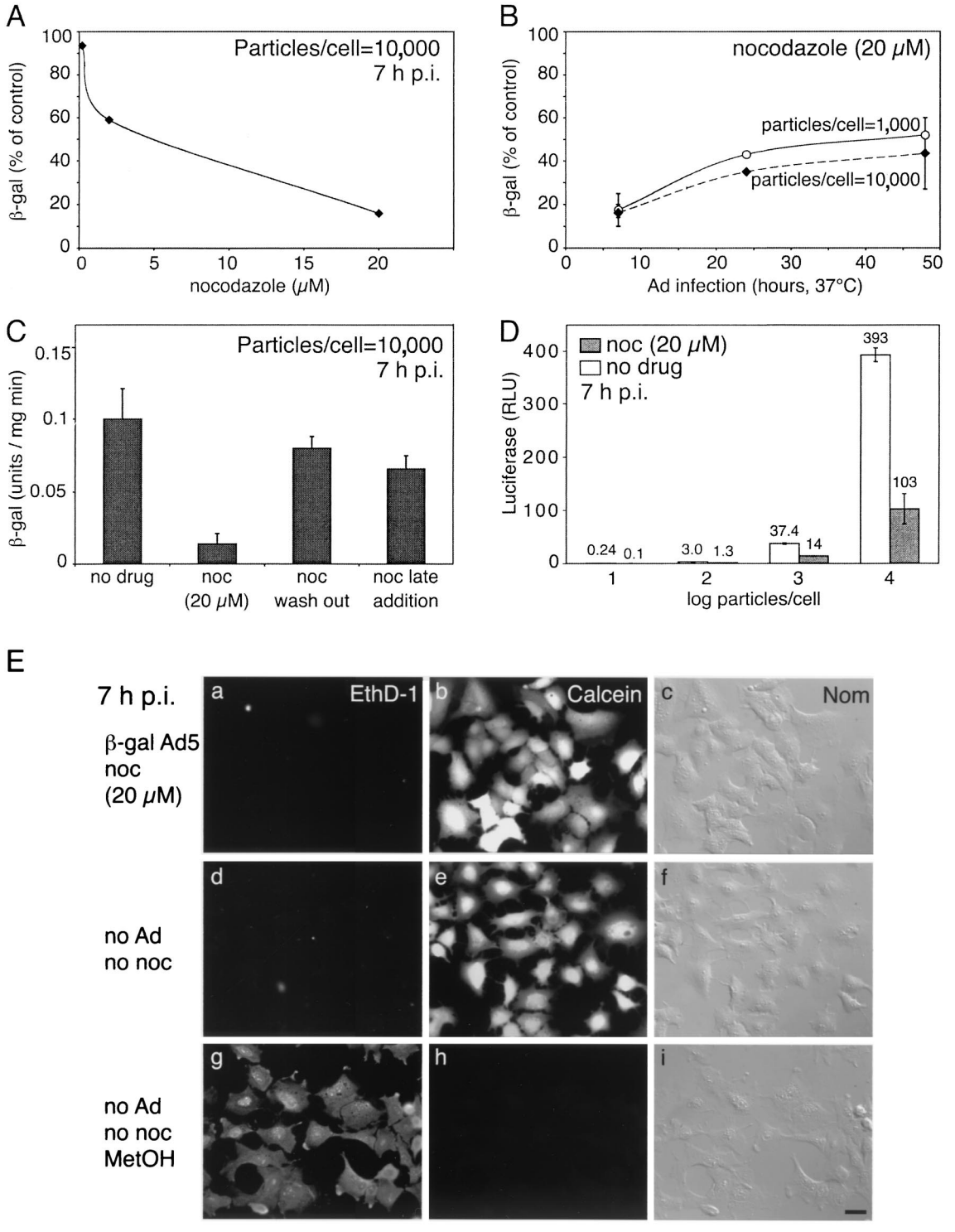

FIG. 1. Ad5-mediated gene expression requires intact MTs. (A to D) A549 cells were not treated or treated with the indicated concentrations of NOC for 1 h and then infected with β-Gal–Ad5 (A to C) or Luc-Ad5 (D) for the indicated times at 37°C. Gene expression was normalized to that of drug-free infected cells (A and B) or is reported as enzymatic units per milligram of protein per minute (C) or relative light units (D) at room temperature. The reversibility of the effects of NOC was tested by washing out the drug at 180 min, and the postentry effects of NOC were assessed by adding the drug at 180 min p.i. (C). Error bars indicate standard errors of the means. (E) Toxicity of NOC for β-Gal–Ad5-infected cells (a to c) and noninfected cells (d to f) at 7 h p.i. with ethidium bromide (a, d, and g) and calcein (b, e, and h) staining and with Nomarksi (Nom) differential interference contrast imaging (c, f, and i). Note that dead cells were EthD-1 positive and calcein negative; see, e.g., methanol (MetOH, 70% for 30 min)-treated cells (g to i). NOC-treated or infected cells were all alive. Bar, 40 μm.

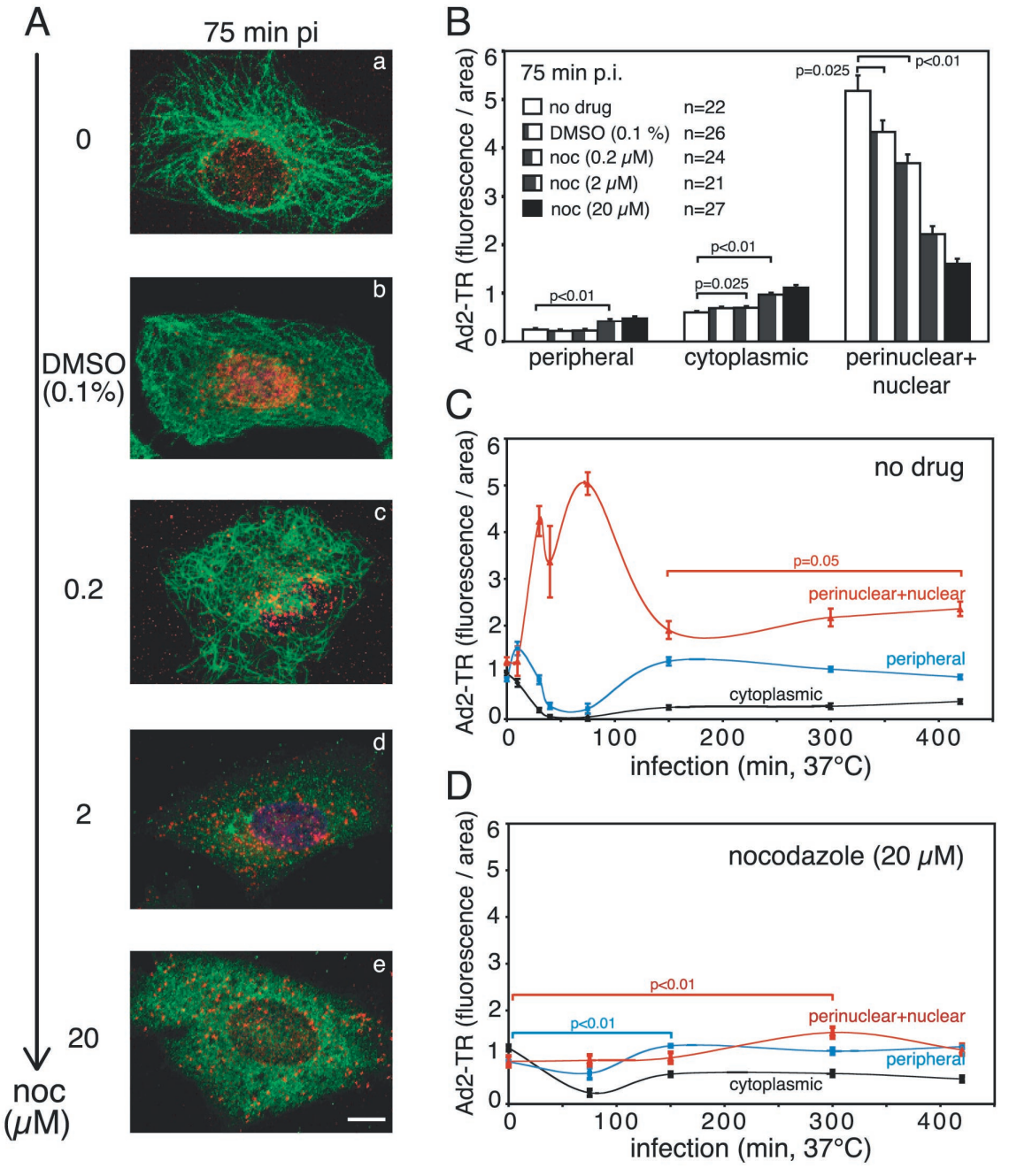

FIG. 2. NOC blocks nuclear targeting of Ad2-TR in A549 cells. Ad2-TR was cold bound to A549 cells not pretreated or pretreated with different concentrations of NOC. Cells were warmed for the indicated times at 37°C in the presence or in the absence of NOC and then fixed with PHEMO-fix. (A) Entire set of projected confocal laser scanning microscopy sections of representative cells depicting Ad2-TR (red), MTs (green), and the nucleus (4′,6′-diamidino-2-phenylindole; dark blue). Note the disappearance of the MTs with increasing concentrations of NOC and the lack of nuclear accumulation of Ad2-TR. Bar, 10 μm. (B) Quantification of the subcellular localization of Ad2-TR in the periphery, the cytoplasm, and the nuclear and perinuclear region of cells treated with different concentrations of NOC (n, number of cells analyzed). (C) Quantification of the subcellular localization of Ad2-TR in A549 control cells over time. Note that the nuclear transport of Ad2-TR peaks at 80 to 90 min p.i., with corresponding reductions in peripheral and cytoplasmic particles. (D) Quantification of the subcellular localization of Ad2-TR in the absence of MTs (NOC treatment). Note the lack of nuclear transport at times before 200 min p.i. and the slight increase in nuclear accumulation at 300 min p.i. Error bars indicate standard errors of the means.

ently reached the nucleus in the absence of MTs. At least some nuclear capsids must have been genome-containing particles, since we detected viral gene expression in the presence of NOC. The reduction in the nuclear capsid signal at 420 min p.i. might have been due to capsid disassembly. In summary, these results indicate that more than 90% of the incoming Ad2-TR did not reach the nucleus in the absence of MTs and that this transport block strongly reduced viral gene expression.

NOC blocks HSV-1-mediated gene expression. MTs are a major intracellular trafficking route of alphaherpesviruses. We therefore tested the effect of NOC on HSV-1 gene delivery using the expression of β-Gal activity controlled by the viral immediate-early promoter of ICP4. PtK_2 cells were pretreated with different concentrations of NOC, incubated with HSV-1 [KOS]tk12 in the cold, infected in the presence or in the absence of drug at 37°C for 4 h, and analyzed for β-Gal activity. The results clearly indicate that NOC is a dose-dependent inhibitor of HSV-1 infection (Fig. 3A). The maximal inhibition of approximately 90% was obtained with 25 μM NOC. This effect was due neither to cell loss, as indicated by cell quantification with crystal violet, nor to cell death, as measured by the live/dead assay (data not shown). We next analyzed the effect of 25 μM NOC on HSV-1 infection in a time course experiment at multiplicities of infection (MOIs) of 2 and 10 from 3 to 7 h p.i. Under all conditions, NOC inhibited viral gene expression in the range of 80 to 90% (Fig. 3B). However, the inhibition was not complete. At an MOI of 10, there was a modest increase in gene expression from 3 to 7 h p.i., indicating that a small fraction of infectious virus had reached the nucleus independently of MTs.

NOC inhibits nuclear targeting of incoming HSV-1. We next tested to what extent NOC affected MTs. Vero cells were preincubated with different concentrations of NOC for 1 h, incubated in the cold with HSV-1, and warmed in the presence or in the absence of drug for 2 h. The highest concentration of NOC (20 μM) completely depolymerized MTs and led to a random cytoplasmic localization of HSV-1 capsids (Fig. 4A, panel d). In the absence of drug, however, the MT network was intact and incoming HSV-1 localized predominantly to the nucleus (Fig. 4A, panel a). Intermediate concentrations of NOC (0.4 and 2 μM) had partial effects on MTs and HSV-1 nuclear targeting (Fig. 4A, panels b and c).

To assess the effect of NOC on the subcellular trafficking of HSV-1, we quantitated viral capsid fluorescence in the periphery, the cytoplasm, and the nuclear and perinuclear region by using the same method as that used for Ad2-TR. In the absence of drug, there was a strong enrichment of HSV-1 near the nucleus and a significant decrease in the peripheral and cytoplasmic viral load at 120 and 180 min p.i. ($P < 0.01$) (Fig. 4B). NOC, however, blocked the nuclear accumulation as well as the cytoplasmic reduction of HSV-1 at 120 and 180 min p.i., compared to the results obtained at 30 min p.i., but did not affect the reduction of virus in the periphery (Fig. 4C). These results suggested that viral trafficking through the cortex was independent of MTs, unlike further cytoplasmic transport, which largely required intact MTs. This conclusion was further supported by experiments with the MT-stabilizing drug paclitaxel (10 μM), which allowed a strong enrichment of HSV-1 near the nucleus, although this enrichment was slightly less pronounced than that in drug-free cells. Accordingly, paclitaxel had only minimal effects on the expression of β-Gal (average inhibition, 20 to 30%). Significantly, paclitaxel did not inhibit the transport of virus through the cell periphery (Fig. 4D). We conclude that HSV-1 capsid transport occurs on stabilized MTs, suggesting that it does not depend on MT treadmilling or dynamic instability.

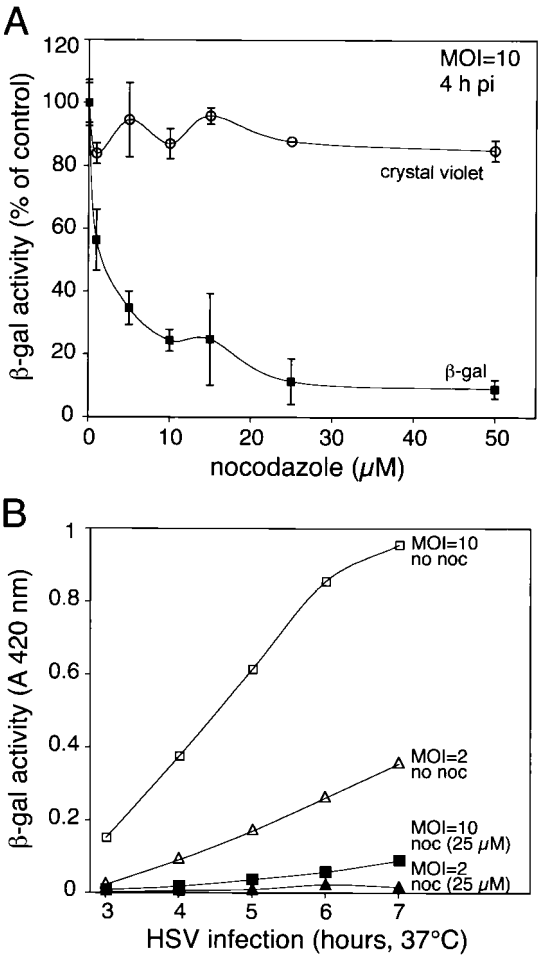

FIG. 3. Intact MTs are required for HSV-1 mediated gene expression. (A) PtK_2 cells were treated with DMSO (control) or NOC for 1 h at 37°C and then incubated with the β-Gal-expressing HSV-1 strain [KOS]tk12 at 4°C for 2 h (MOI, 10). The unbound viruses were removed, and the cells were shifted to 37°C in the presence or in the absence of NOC to initiate infection. Cells were lysed at 4 h p.i., and the amount of β-Gal was quantitated (squares). Cells on parallel dishes were quantified by using the binding of crystal violet (circles). The means and standard deviations for duplicate samples are shown. Note that with increasing NOC concentrations, the amount of immediate-early viral gene expression was inhibited. (B) Time course of HSV-1 gene expression. Cells were infected in the absence (filled symbols) or in the presence (open symbols) of MTs with HSV-1 [KOS]tk12 (MOI of 2 [triangles] or MOI of 10 [squares]), lysed at different times p.i., and analyzed for β-Gal expression (absorbance at 420 nm). At both MOIs and at all times tested, NOC clearly reduced immediate-early viral gene expression. The crystal violet assay showed no significant loss of cells under these conditions (<5%) (data not shown).

DISCUSSION

Using quantitative subcellular localization of incoming viral capsids and quantification of viral gene expression in the absence or in the presence of NOC, an MT-depolymerizing agent, we found that MTs play a crucial role in delivering Ad and HSV-1 genomes to the nuclei of epithelial cells. The NOC inhibition was reversible (45, 49; this study), NOC had no effect on cellular gene expression (data not shown), and only minor

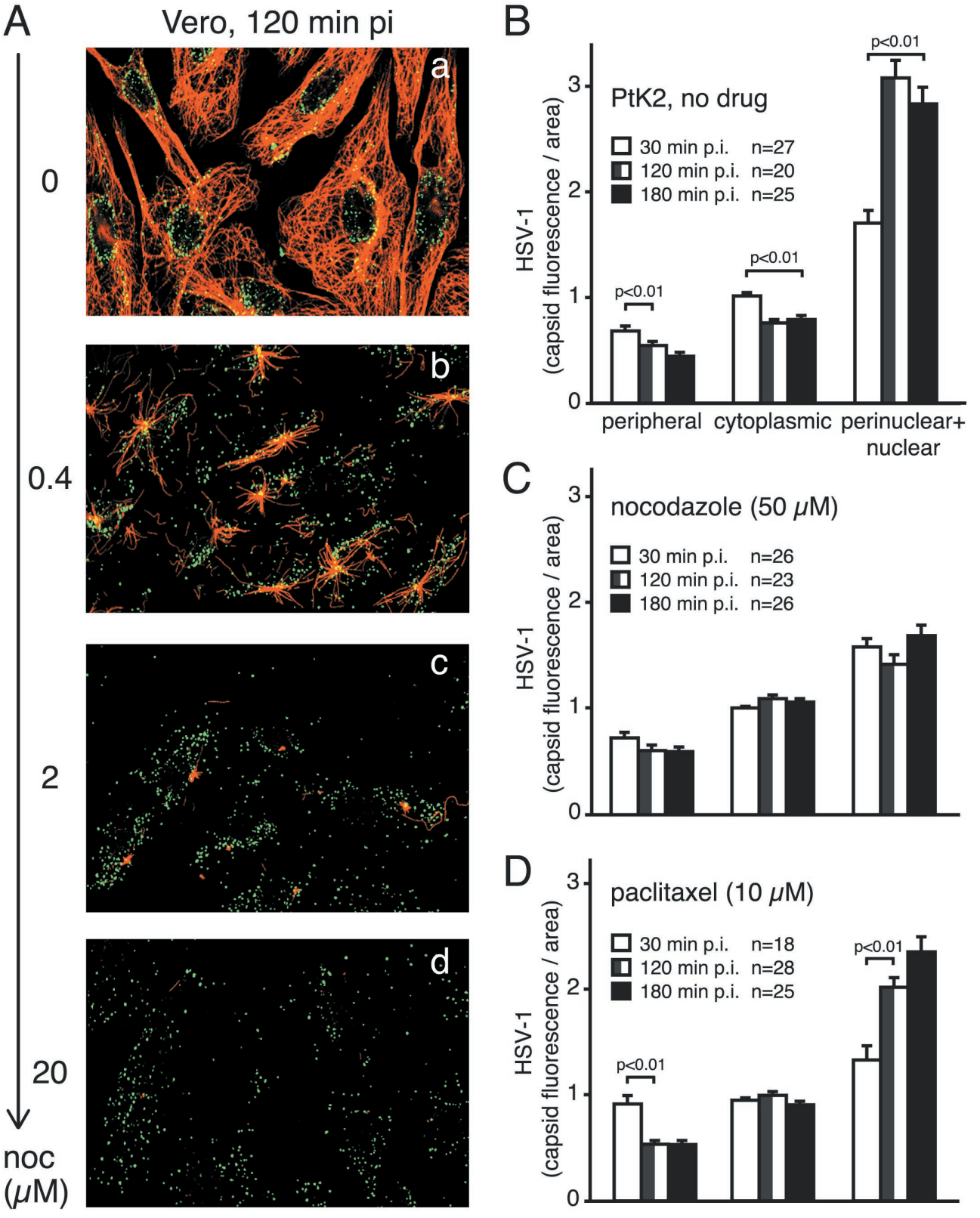

FIG. 4. NOC inhibits the nuclear targeting of HSV-1 in Vero and PtK_2 cells. (A) Vero cells were infected in the absence or in the presence of different concentrations of NOC with 50 PFU of HSV-1 per cell for 2 h and then fixed in methanol after preextraction. Samples were stained with anti-HC (green) and antitubulin (red) and analyzed by confocal laser scanning microscopy. Note the disappearance of the MTs with increasing concentrations of NOC and the lack of nuclear HSV-1 capsids. (B to D) Quantification of subcellular localization of HSV-1 in PtK_2 cells infected with 80 PFU per cell in the absence of drug (B), in the presence of 50 μM NOC (C), or in the presence of 10 μM paclitaxel (D). Cells were fixed at 30, 120, or 180 min p.i. and labeled with anti-LC. n, number of cells. Error bars indicate standard errors of the means. MTs in Vero cells were completely depolymerized at lower concentrations of NOC than were those in PtK_2 cells (data not shown).

effects on viral gene expression after particle transport to the nucleus had occurred (this study). We therefore concluded, as others have before, that NOC is not a general inhibitor of transcription or translation but acts predominantly on the MT network (20).

MTs are required for viral capsid transport. There are several explanations for why NOC treatment did not completely inhibit the delivery of viral DNA into the nucleus. Virions can enter from the plasma membrane proximal to the nuclear envelope. These particles are separated from the nucleus by only a few micrometers. Another possibility is that cytosolic virions use an MT-independent transport mechanism, such as an actin-based system (36, 38); that they are transported on short, randomly oriented MT filaments resistant to NOC; or that they exploit diffusion. All of these processes would stop when the capsid binds to the NPC, leading to particle enrichment at the nucleus. Clearly, Ad2-TR particles are able to explore a few micrometers of cytosolic space in the absence of MTs (8, 49); thus, particles entering from the plasma membrane proximal to the nucleus will most likely not require MTs to reach the NPC. This means that careful kinetic measurements are necessary to reveal the role of any cytoplasmic transport system.

We predict that cells that are particularly small will be infected in the absence of MTs if enough time is allowed. This scenario may, in fact, have obscured the role of MTs in Ad infection (5, 50). Our measurements here reveal that nuclear transport of both Ad2 and HSV-1 from distal areas to the nucleus is blocked in the absence of MTs. Since HSV-1 infection of polarized neuronal cells in a compartmentalized culture absolutely depends on MTs (22), the results obtained with HSV-1 confirm that the quantitative imaging procedures that we used for Ad2 and HSV-1 are reliable. The role of MTs in cytoplasmic particle trafficking is in agreement with the results of studies of endocytic and exocytic membrane traffic and axonal transport, where NOC was found to be a kinetic rather than an absolute inhibitor of membrane traffic (9, 24).

Capsid transport and viral gene expression required neither MT treadmilling nor the dynamic instability of MTs, since paclitaxel (at concentrations of 180 nM to 10 μM) had only slight effects on Ad2 and HSV-1 infections. Likewise, cells expressing MAP4, which stabilizes the MT network (34), transported Ad2 to the nucleus even faster than control cells (49); low concentrations of paclitaxel or NOC (5 nM), suppressing MT dynamics without depolymerizing MTs, have similar effects (6, 7). Thus, preferentially stabilized MTs effectively support viral transport to the nucleus. A further indication that Ad2 utilizes MTs for nuclear targeting came from experiments in which transport directionality was controlled. Ad2 was found to stimulate two distinct signaling pathways which both enhance the MT-dependent minus-end-directed transport of Ad2 capsids (48). In the absence of stimulation, viral motility was directed toward the cell periphery, dependent on intact MTs.

Live imaging of MT-dependent and independent Ad transport. Glotzer et al. (8) recently questioned the role of MTs in Ad5 infection. They traced incoming Ad5 that contained a GFP-tetracycline repressor fusion protein (GFP-TetR) bound to operator sequences in the Ad5 DNA genome but were not able to detect fast retrograde motions of GFP-TetR-tagged Ad5, unlike other reports with fluorophore-tagged Ad (26, 48, 49).

There are several not mutually exclusive possibilities for why Glotzer et al. (8) missed the fast minus-end-directed motility of Ad. The first possibility involves temperature. Glotzer et al. (8) used room temperature for their live experiments, whereas we always conducted our live experiments at 37°C with a temperature-controlled sample holder. The second possibility involves longer intervals between subsequent frames. While we recorded frame intervals of 1 to 2 s, Glotzer et al. (8) used frame intervals of 3 to 5 s. Longer intervals make it less likely that high-speed elementary motion steps will be detected. The third possibility involves imaging with PBS. For their tracing experiments, Glotzer et al. (8) used PBS lacking glucose and other nutrients, whereas we used growth medium without serum (and sometimes also without phenol red). Depending on the duration of the incubation, PBS may reduce the ATP levels in the cells. Interestingly, the vast majority of the particles (about 15 to 20 particles, corresponding to about 95%) in the study of Glotzer et al. (8) were apparently nonmotile during the 14-s period depicted in their Fig. 4A. This result is again in contrast to our imaging of 40 to 60% motile particles (7, 48, 49). The fourth possibility involves imaging at shorter wavelengths and longer exposure times. Glotzer et al. (8) used GFP-tagged Ad and thus had to use an excitation beam of about 500 nm. Their exposure times were between 1 and 1.5 s, whereas our exposure times were between 0.2 and 0.4 s, i.e., four or five times shorter and thus less phototoxic. The published images in the study of Glotzer et al. (8) demonstrate photobleaching effects after as few as five frames (their Fig. 4A). Phototoxicity is known to affect the viability of cells; thus, their results are difficult to compare with our data. We imaged the TR fluorophore with a 595-nm excitation and were able to record several hundred subsequent frames (48, 49). The fifth possibility involves statistical analysis. Due to the limited data set that Glotzer et al. (8) were able to collect, their statistical analysis was limited. They processed between 20 and 218 frames per assay, whereas we included several thousand frames per assay. Thus, our standard deviations of the mean are smaller and the differences between various conditions (e.g., plus or minus NOC) are highly significant for our measurements (one-sided *t* tests). The sixth possibility involves the subcellular area of particle tracing. Figure 4 in the study of Glotzer et al. (8) shows that 8 out of 11 traced particles were in a region proximal to the nucleus, i.e., separated by less than 10 μm from the nuclear envelope. The perinuclear region is known to be elevated compared to the flat periphery. Motility in this region can also occur along the *z* axis and thus toward and away from the detector; i.e., the observed velocities in the perinuclear region might have been underestimated. Many studies, including ours, have therefore traced organelles (23) and viruses (reviewed in reference 12) in the peripheral flat regions of the cytoplasm and have used cells that are extensively spread out (see, e.g., reference 30). The final possibility involves the nature of GFP-TetR-tagged Ad particles. Glotzer et al. (8) used GFP-TetR-tagged Ad5 in which GFP-TetR was bound to operator sequences in the genomic DNA. Using biochemical assays, they demonstrated that the tag cofractionated with a viral DNA binding protein at 30 min p.i., but the stability of this interaction later in infection was not characterized. It is also unclear

what fraction of the particles was recovered in their analysis at 30 min p.i., since the control fractionation sample at 0 min p.i. was missing. They then performed all their fluorescence motility experiments at times between 30 and 80 min p.i.; thus, it is unknown whether the tag was in fact still on the viral particle. That the tag could prematurely dissociate from the DNA was suggested by their observations that GFP-TetR was not found to be imported into the nucleus but that viral DNA was apparently imported. In addition, it is not known whether the tagged DNA was completely packaged into the virion. If packaging was incomplete, then it is possible that some of the DNA dissociated from the capsid prior to capsid arrival at the nucleus. The dissociated DNA might or might not have been tagged with GFP-TetR and thus might have appeared as fluorescent puncta. It is likely that these puncta would have had motilities different from those of our Ad2-TR.

Besides these important technical differences in the live fluorescence experiments, another major difference between the study of Glotzer et al. (8) and our study is the effect of NOC on the movement of particles to the nucleus. Glotzer et al. (8) found no effect of NOC on the movement of GFP-TetR-tagged Ad DNA. Given the limitations of their tracing experiments, this result is not surprising. Glotzer et al. (8) measured slow short-range transport in both control and NOC-treated cells, i.e., MT-independent transport. Their static analysis, however, showed that GFP-TetR-tagged particles were found at the microtubule organizing center at 30 to 40 min p.i. when MTs were present but not when they were absent. This finding fully agrees with our findings and further supports the notion that the live analyses of Glotzer et al. (8) had technical limitations obscuring the detection of fast motility steps.

It is important that the fluorescent dots that we detected with Ad2-TR correspond to single viral particles that have the same infectivity as their "parental" nonlabeled particles (33). Quantitative subcellular localization of capsids in static images indicated that in control cells, about 65% of the Ad2-TR accumulates over the nuclear and perinuclear region at 90 min p.i. (33). This finding is in good agreement with the Ad2-TR motilities in epithelial and fibroblastic cells (e.g., HeLa cells, rat kangaroo PtK_2 cells, African green monkey TC7 cells, or mouse embryo fibroblasts), which are biased toward the nucleus and have net population speeds on the order of several micrometers per minute (48, 49). Elementary motility events were between 0.2 and 0.4 μm/s and reached minus-end-directed peak velocities of up to 2.6 μm/s. Moreover, capsids were transported over short ranges as well as long distances, consistent with processive motor-driven motility. Overexpression of the p50 subunit of the dynactin complex or antidynein antibodies indicated that the minus-end-directed MT motor complex dynein-dynactin has a key function in transporting Ad2 as well as HSV-1 to the nucleus (6a, 26, 49). We conclude that MTs are instrumental for the trafficking of Ad2 and HSV-1 particles to the nucleus.

NOC inhibits Ad and HSV-1 infections. Consistent with a role of MTs in transporting infectious DNA to the nucleus, we found viral gene expression to be significantly inhibited in cells lacking MTs. These cells remained on the substratum and showed no signs of leakiness, i.e., cell death. With different viruses (Ad2, Ad5, and HSV-1), different cell lines (Vero, PtK_2, A549, and HeLa), different MT-depolymerizing agents (vinblastine [45] and NOC [this study]), different genes (ICP4, β-Gal, and luciferase [45; this study]), different promoters (HSV-1 ICP4 and CMV immediate early), and different MOIs (from 2 to 100 PFU/cell), viral gene expression was in all instances found to be inhibited by 50 to 90%.

Our results again contrast those of Glotzer et al. (8). These authors reported data suggesting that NOC had no effect on the expression of luciferase from transgenic Ad5 or on infection, as estimated by counting of immunostained cells expressing the immediate-early viral protein E1A. NOC also appeared to have no effect on GFP expression encoded by Ad5, as determined by counting of green fluorescent cells. While the percentage of fluorescent cells can be easily determined, the fluorescent signal may not be linear over a wide range of protein concentrations. Measuring an enzymatic activity, such as luciferase or β-Gal, however, allows for unambiguous quantification if the assay is performed within the linear range of the enzymatic activity. Glotzer et al. (8) reported that 1,000 particles per cell gave an average of about 10^2 luciferase light units at 4 h p.i., whereas 10 times as much virus (10,000 particles per cell) resulted in 5×10^4 light units. This value is 50-fold more than what would be expected if the measurements followed linear kinetics. Moreover, there was essentially no increase in the luciferase signal from 6 to 24 h p.i. with 10,000 particles per cell, suggesting that the assay had been saturated.

In summary, we conclude that intact MTs and their associated motors support the transport of infectious Ad and HSV-1 particles to the nucleus and thereby enhance the kinetics of infection. Based on earlier results (14, 15, 35, 45, 53), we argue that the Ad and HSV-1 genomes remain enclosed in capsids during their cytosolic passage to the nucleus. Only when these capsids arrive at the NPC will they be disassembled and their DNA released and imported into the nucleus for transcription and replication.

ACKNOWLEDGMENTS

Hélène Mabit and Michel Y. Nakano contributed equally to this work.

We thank S. Hemmi and D. Serena for generous gifts of Luc-Ad5, I. Vigne and P. Yeh for Ad5 derivative AE18, P. Spear for HSV-1 [KOS]tk12, R. Eisenberg and G. Cohen for antibodies against HSV-1 capsids, R. Stidwill and P. Groscurth for confocal laser scanning microscopy imaging, and D. Meder (Hannover, Germany) for assistance with the β-Gal assay.

This work was supported by the Swiss National Science Foundation and the Kanton Zürich (support given to U.F.G.), as well as by the German Research Council (DFG; grant SO403-1 to B.S.).

REFERENCES

1. **Bearer, E. L., X. O. Breakefield, D. Schuback, T. S. Reese, and J. H. LaVail.** 2000. Retrograde axonal transport of herpes simplex virus: evidence for a single mechanism and a role for tegument. Proc. Natl. Acad. Sci. USA **97:**8146–8150.
2. **Blose, S. H., D. I. Meltzer, and J. R. Feramisco.** 1984. 10-nm filaments are induced to collapse in living cells microinjected with monoclonal and polyclonal antibodies against tubulin. J. Cell Biol. **98:**847–858.
3. **Chartier, C., E. Degryse, M. Gantzer, A. Dieterle, A. Pavirani, and M. Mehtali.** 1996. Efficient generation of recombinant adenovirus vectors by homologous recombination in *Escherichia coli*. J. Virol. **70:**4805–4810.
4. **Cohen, G. H., M. Ponce de Leon, H. Diggelmann, W. C. Lawrence, S. K. Vernon, and R. J. Eisenberg.** 1980. Structural analysis of the capsid polypeptides of herpes simplex virus types 1 and 2. J. Virol. **34:**521–531.
5. **Dales, S., and Y. Chardonnet.** 1973. Early events in the interaction of adenoviruses with HeLa cells. IV. Association with microtubules and the nuclear pore complex during vectorial movement of the inoculum. Virology **56:**465–483.

6. **Derry, W. B., L. Wilson, and M. A. Jordan.** 1995. Substoichiometric binding of taxol suppresses microtubule dynamics. Biochemistry **34:**2203–2211.

6a. **Döhner, K., A. Wolfstein, J. Prank, C. Echeverri, D. Dujardin, R. Vallee, and B. Sodeik.** 2002. Function of dynein and dynactin in herpes simplex capsid transport. Mol. Biol. Cell **13:**2559–2573.

7. **Giannakakou, P., M. Y. Nakano, K. C. Nicolaou, A. O'Brate, J. Yu, M. V. Blagosklonny, U. F. Greber, and T. Fojo.** 2002. Enhanced microtubule-dependent trafficking and p53 nuclear accumulation by suppression of microtubule dynamics. Proc. Natl. Acad. Sci. USA **99**:10855–10860.

8. **Glotzer, J. B., A. I. Michou, A. Baker, M. Saltik, and M. Cotten.** 2001. Microtubule-independent motility and nuclear targeting of adenoviruses with fluorescently labeled genomes. J. Virol. **75:**2421–2434.

9. **Goldstein, L. S., and Z. Yang.** 2000. Microtubule-based transport systems in neurons: the roles of kinesins and dyneins. Annu. Rev. Neurosci. **23:**39–71.

10. **Granzow, H., F. Weiland, A. Jons, B. G. Klupp, A. Karger, and T. C. Mettenleiter.** 1997. Ultrastructural analysis of the replication cycle of pseudorabies virus in cell culture: a reassessment. J. Virol. **71:**2072–2082.

11. **Greber, U. F.** 2002. Signalling in viral entry. Cell Mol. Life Sci. **59:**608–626.

12. **Greber, U. F., and E. Carafoli.** 2002. Signalling takes control of nucleocytoplasmic transport. EMBO Rep. **3:**410–414.

13. **Greber, U. F., M. Y. Nakano, and M. Suomalainen.** 1998. Adenovirus entry into cells: a quantitative fluorescence microscopy approach. Methods Mol. Med. **21:**217–230.

14. **Greber, U. F., M. Suomalainen, R. P. Stidwill, K. Boucke, M. Ebersold, and A. Helenius.** 1997. The role of the nuclear pore complex in adenovirus DNA entry. EMBO J. **16:**5998–6007.

15. **Greber, U. F., P. Webster, J. Weber, and A. Helenius.** 1996. The role of the adenovirus protease in virus entry into cells. EMBO J. **15:**1766–1777.

16. **Greber, U. F., M. Willetts, P. Webster, and A. Helenius.** 1993. Stepwise dismantling of adenovirus 2 during entry into cells. Cell **75:**477–486.

17. **Hammonds, T. R., S. P. Denyer, D. E. Jackson, and W. L. Irving.** 1996. Studies to show that with podophyllotoxin the early replicative stages of herpes simplex virus type 1 depend upon functional cytoplasmic microtubules. J. Med. Microbiol. **45:**167–172.

18. **Horwitz, M. S.** 1990. Adenoviridae and their replication, p. 1679–1721. *In* B. N. Fields and D. M. Knipe (ed.), Virology, 2nd ed., vol. 1. Raven Press, New York, N.Y.

19. **Horwitz, M. S.** 1996. Adenoviruses, p. 2149–2171. *In* B. N. Fields, D. M. Knipe, and P. M. Howley (ed.), Fields virology, 3rd ed., vol. 1. Raven Press, Philadelphia, Pa.

20. **Jordan, M. A., and L. Wilson.** 1999. The use and action of drugs in analyzing mitosis. Methods Cell Biol. **61:**267–295.

21. **Kay, M. A., J. C. Glorioso, and L. Naldini.** 2001. Viral vectors for gene therapy: the art of turning infectious agents into vehicles of therapeutics. Nat. Med. **7:**33–40.

22. **Kristensson, K., E. Lycke, M. Roytta, B. Svennerholm, and A. Vahlne.** 1986. Neuritic transport of herpes simplex virus in rat sensory neurons in vitro. Effects of substances interacting with microtubular function and axonal flow [nocodazole, taxol and erythro-9-[3-(2-hydroxynonyl)]adenine]. J. Gen. Virol. **67:**2023–2028.

23. **Künzi, V., M. Glatzel, M. Y. Nakano, U. F. Greber, F. van Leuwen, and A. Aguzzi.** Unhampered prion neuroinvasion despite impaired fast axonal transport in transgenic mice overexpressing four-repeat tau. J. Neurosci., in press.

24. **Lane, J., and V. Allan.** 1998. Microtubule-based membrane movement. Biochim. Biophys. Acta **1376:**27–55.

25. **Leopold, P. L., B. Ferris, I. Grinberg, S. Worgall, N. R. Hackett, and R. G. Crystal.** 1998. Fluorescent virions—dynamic tracking of the pathway of adenoviral gene transfer vectors in living cells. Hum. Gene Ther. **9:**367–378.

26. **Leopold, P. L., G. Kreitzer, N. Miyazawa, S. Rempel, K. K. Pfister, E. Rodriguez-Boulan, and R. G. Crystal.** 2000. Dynein- and microtubule-mediated translocation of adenovirus serotype 5 occurs after endosomal lysis. Hum. Gene Ther. **11:**151–165.

27. **Luftig, R. B., and R. R. Weihing.** 1975. Adenovirus binds to rat brain microtubules in vitro. J. Virol. **16:**696–706.

28. **Lycke, E., K. Kristensson, B. Svennerholm, A. Vahlne, and R. Ziegler.** 1984. Uptake and transport of herpes simplex virus in neurites of rat dorsal root ganglia cells in culture. J. Gen. Virol. **65:**55–64.

29. **Markert, J. M., M. D. Medlock, S. D. Rabkin, G. Y. Gillespie, T. Todo, W. D. Hunter, C. A. Palmer, F. Feigenbaum, C. Tornatore, F. Tufaro, and R. L. Martuza.** 2000. Conditionally replicating herpes simplex virus mutant, G207 for the treatment of malignant glioma: results of a phase I trial. Gene Ther. **7:**867–874.

30. **Matteoni, R., and T. E. Kreis.** 1987. Translocation and clustering of endosomes and lysosomes depends on microtubules. J. Cell Biol. **105:**1253–1265.

31. **Miles, B. D., R. B. Luftig, J. A. Weatherbee, R. R. Weihing, and J. Weber.** 1980. Quantitation of the interaction between adenovirus types 2 and 5 and microtubules inside infected cells. Virology **105:**265–269.

32. **Miyazawa, N., R. G. Crystal, and P. L. Leopold.** 2001. Adenovirus serotype 7 retention in a late endosomal compartment prior to cytosol escape is modulated by fiber protein. J. Virol. **75:**1387–1400.

33. **Nakano, M. Y., and U. F. Greber.** 2000. Quantitative microscopy of fluorescent adenovirus entry. J. Struct. Biol. **129:**57–68.

34. **Nguyen, H. L., S. Chari, D. Gruber, C. M. Lue, S. J. Chapin, and J. C. Bulinski.** 1997. Overexpression of full- or partial-length Map4 stabilizes microtubules and alters cell growth. J. Cell Sci. **110:**281–294.

35. **Ojala, P. M., B. Sodeik, M. W. Ebersold, U. Kutay, and A. Helenius.** 2000. Herpes simplex virus type 1 entry into host cells: reconstitution of capsid binding and uncoating at the nuclear pore complex in vitro. Mol. Cell. Biol. **20:**4922–4931.

36. **Pantaloni, D., C. Le Clainche, and M. F. Carlier.** 2001. Mechanism of actin-based motility. Science **292:**1502–1506.

37. **Penfold, M. E., P. Armati, and A. L. Cunningham.** 1994. Axonal transport of herpes simplex virions to epidermal cells: evidence for a specialized mode of virus transport and assembly. Proc. Natl. Acad. Sci. USA **91:**6529–6533.

38. **Ploubidou, A., and M. Way.** 2001. Viral transport and the cytoskeleton. Curr. Opin. Cell Biol. **13:**97–105.

39. **Ries, S., and W. M. Korn.** 2002. ONYX-015: mechanisms of action and clinical potential of a replication-selective adenovirus. Br. J. Cancer **86:**5–11.

40. **Roizman, B., and D. M. Knipe.** 2001. Herpes simplex viruses and their replication, p. 1123–1183. *In* D. M. Knipe and P. M. Howley (ed.), Fundamental virology, 4th ed. Lippincott-Raven, Philadelphia, Pa.

41. **Segerman, A., Y. F. Mei, and G. Wadell.** 2000. Adenovirus types 11p and 35p show high binding efficiencies for committed hematopoietic cell lines and are infective to these cell lines. J. Virol. **74:**1457–1467.

42. **Seth, P., M. C. Willingham, and I. Pastan.** 1985. Adenovirus-dependent release of ^{51}Cr from KB cells at an acidic pH. J. Biol. Chem. **259:**14350–14353.

43. **Smith, G. A., S. P. Gross, and L. W. Enquist.** 2001. Herpesviruses use bidirectional fast-axonal transport to spread in sensory neurons. Proc. Natl. Acad. Sci. USA **98:**3466–3470.

44. **Sodeik, B.** 2000. Mechanisms of viral transport in the cytoplasm. Trends Microbiol. **8:**465–472.

45. **Sodeik, B., M. W. Ebersold, and A. Helenius.** 1997. Microtubule-mediated transport of incoming herpes simplex virus 1 capsids to the nucleus. J. Cell Biol. **136:**1007–1021.

46. **Spear, P. G., R. J. Eisenberg, and G. H. Cohen.** 2000. Three classes of cell surface receptors for alphaherpesvirus entry. Virology **275:**1–8.

47. **Stidwill, R. S., and U. F. Greber.** 2000. Intracellular virus trafficking reveals physiological characteristics of the cytoskeleton. News Physiol. Sci. **15:**67–71.

48. **Suomalainen, M., M. Y. Nakano, K. Boucke, S. Keller, and U. F. Greber.** 2001. Adenovirus-activated PKA and p38/MAPK pathways boost microtubule-mediated nuclear targeting of virus. EMBO J. **20:**1310–1319.

49. **Suomalainen, M., M. Y. Nakano, K. Boucke, S. Keller, R. P. Stidwill, and U. F. Greber.** 1999. Microtubule-dependent minus and plus end-directed motilities are competing processes for nuclear targeting of adenovirus. J. Cell Biol. **144:**657–672.

50. **Svensson, U., and R. Persson.** 1984. Entry of adenovirus 2 into HeLa cells. J. Virol. **51:**687–694.

51. **Topp, K. S., K. Bisla, N. D. Saks, and J. H. Lavail.** 1996. Centripetal transport of herpes simplex virus in human retinal pigment epithelial cells in vitro. Neuroscience **71:**1133–1144.

52. **Topp, K. S., L. B. Meade, and J. H. LaVail.** 1994. Microtubule polarity in the peripheral processes of trigeminal ganglion cells: relevance for the retrograde transport of herpes simplex virus. J. Neurosci. **14:**318–325.

53. **Trotman, L. C., N. Mosberger, M. Fornerod, R. P. Stidwill, and U. F. Greber.** 2001. Import of adenovirus DNA involves the nuclear pore complex receptor CAN/Nup214 and histone H1. Nat. Cell Biol. **3:**1092–1100.

54. **Vigne, E., I. Mahfouz, J. F. Dedieu, A. Brie, M. Perricaudet, and P. Yeh.** 1999. RGD inclusion in the hexon monomer provides adenovirus type 5-based vectors with a fiber knob-independent pathway for infection. J. Virol. **73:**5156–5161.

55. **Wagner, E. K., and D. C. Bloom.** 1997. Experimental investigation of herpes simplex virus latency. Clin. Microbiol. Rev. **10:**419–443.

56. **Warner, M. S., R. J. Geraghty, W. M. Martinez, R. I. Montgomery, J. C. Whitbeck, R. L. Xu, R. J. Eisenberg, G. H. Cohen, and P. G. Spear.** 1998. A cell surface protein with herpesvirus entry activity (Hveb) confers susceptibility to infection by mutants of herpes simplex virus type 1, herpes simplex virus type 2, and pseudorabies virus. Virology **246:**179–189.

57. **Weatherbee, J. A., R. B. Luftig, and R. R. Weihing.** 1977. Binding of adenovirus to microtubules. II. Depletion of high-molecular-weight microtubule-associated protein content reduces specificity of in vitro binding. J. Virol. **21:**732–742.